Variational methods for characterizing matrix product operator symmetries

Anna Francuz,[1,*] Laurens Lootens,[2] Frank Verstraete,[2] and Jacek Dziarmaga[1]
[1]*Jagiellonian University, Institute of Theoretical Physics, Łojasiewicza 11, PL-30348 Kraków, Poland*
[2]*Department of Physics and Astronomy, Ghent University, Krijgslaan 281, S9, B-9000 Ghent, Belgium*

(Received 28 July 2021; revised 12 November 2021; accepted 18 November 2021; published 29 November 2021)

We present a method of extracting information about topological order from the ground state of a strongly correlated two-dimensional system represented by an infinite projected entangled pair state (iPEPS). As in previous works [A. Francuz *et al.*, Phys. Rev. B **101**, 041108(R) (2020) and A. Francuz and J. Dziarmaga *ibid.* **102**, 235112 (2020)] we begin by determining symmetries of the iPEPS represented by infinite matrix product operators (iMPO) that map between the different iPEPS transfer matrix fixed points, to which we apply the fundamental theorem of matrix product states to find zipper tensors between products of iMPO's that encode fusion properties of the anyons. The zippers can be combined to extract topological F symbols of the underlying fusion category, which unequivocally identifies the topological order of the ground state. We bring the F symbols to the canonical gauge, and also compute the Drinfeld center of this unitary fusion category to extract the topological S and T matrices encoding mutual statistics and self-statistics of the emergent anyons. The algorithm is applied to Abelian toric code, Kitaev model, double semion, and twisted quantum double of Z_3, as well as to non-Abelian double Fibonacci, double Ising, and quantum double of S_3 and Rep(S_3) string-net models.

DOI: 10.1103/PhysRevB.104.195152

I. INTRODUCTION

Topologically ordered phases [1] support anyonic excitations that open the possibility of realizing fault-tolerant quantum computation [2] by braiding of non-Abelian anyons. Aside from the class of exactly solvable models [2–4], verifying if a more general microscopic Hamiltonian has a topologically ordered ground state was traditionally regarded to be an extremely hard task. Recently, observation of quantized Hall effect in Kitaev-type ruthenium chloride α-$RuCl_3$ in magnetic field [5] granted the problem with urgent experimental relevance. Intensive experimental search for other Kitaev-type materials is under way [6].

The density matrix renormalization group (DMRG) [7,8] on a long cylinder used to be the numerical method of choice [9–24]. In the limit of infinitely long cylinders, DMRG naturally produces ground states with well-defined anyonic flux from which one can obtain characterization of a topological order via so-called topological S and T matrices [25]. Since the proposal of Ref. [25], this approach has become a common practice [26–43].

Unfortunately, the cost of a DMRG simulation grows exponentially with the circumference of cylinder, limiting this approach to thin cylinders (up to a circumference of $\simeq$14 sites) and thus to short correlation lengths (up to $\xi = 1 \sim 2$ sites), since the circumference has to be at least $\approx 6\xi$ to reach convergence in the cylinder width. Instead, infinite projected entangled pair states (iPEPS) in principle allow for much longer correlation lengths [44–46]. A unique ground state on an infinite lattice can be represented by an iPEPS that is either a variational ansatz [47] or a result of numerical optimization [48–51].

When wrapped on a cylinder, the iPEPS becomes a superposition of degenerate ground states with definite anyonic fluxes. In the realm of the string-net models it is possible [49,52] to produce a PEPS-like tensor network for each ground state with well-defined flux (see Fig. 1). Such tensor networks are suitable for extracting topological S and T matrices by computing overlaps between the ground states. Furthermore, they allow for computation of topological second Renyi entropy directly in the limit of infinite cylinder's width. The approach of Refs. [49,52] does not assume clean realization of certain symmetries on the bond indices, in contrast to [53–56]. This has been demonstrated in Ref. [49] by examples of toric code and double semions perturbed away from a fixed point towards a ferromagnetic phase as well as for the numerical iPEPS representing the ground state of the Kitaev model in the gapped phase. The same approach was generalized to non-Abelian topological order in Ref. [52]. The method does not require restoring the symmetries by suitable gauge transformations of a numerical iPEPS, a feat that was accomplished in Ref. [57] for the toric code with a perturbation. It is also not necessary to optimize symmetry-constrained iPEPS tensors as in Ref. [58]. Finally, it also has much lower numerical cost than methods based on the tensor renormalization group [59].

In this work we reconsider the string-net models. Similarly as in Refs. [49,52], for a given iPEPS we numerically obtain its infinite matrix product operator (iMPO) symmetries. Products of the iMPO symmetries realize fusion rules of the corresponding anyons of a unitary fusion category (UFC) $\mathcal{C}$.

*Corresponding author: anna.francuz@uj.edu.pl

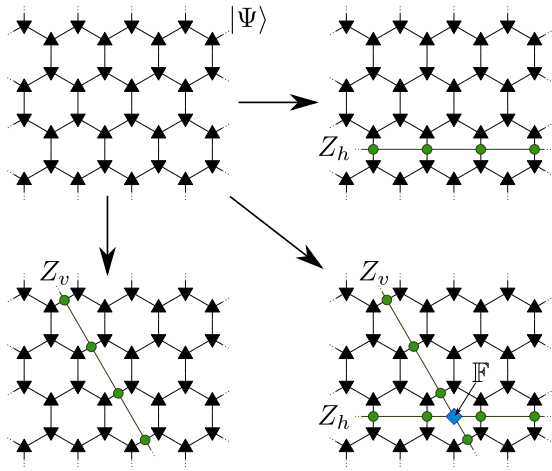

FIG. 1. The method of Refs. [49,52]. From the unique ground state on an infinite lattice, represented by an iPEPS $|\Psi\rangle$, various states inserted with infinite MPO symmetries, Z_h and Z_v, are constructed. Their linear combinations, whose coefficients are determined by fusion rules of the iMPO symmetries (corresponding to anyonic fusion rules), become a basis of states with well-defined anyonic flux. Overlaps of these infinite states determine the topological matrices S and T. Here physical indices are not shown for simplicity.

We use the fundamental theorem of *matrix product states* (MPS) [60,61] and apply it to the iMPO products in order to classify topological order through its related fusion categories. The fundamental theorem of MPS has already been widely used in characterization of phases of both one-dimensional (1D) and two-dimensionl (2D) gapped systems [62,63] as well as the construction of exact renormalization fixed-point representations of string nets with iPEPS [53,54]. The theorem allows us to construct gauge transformations (zippers) between products of iMPO's and their fusion outcomes. The zippers encode information on fusion properties of the corresponding anyons, and they can be combined in order to extract the F symbols of the underlying UFC $\mathcal{C}$ describing the topological order unequivocally. The different ground states and possible anyonic excitations of the string-net model are actually described by the Drinfeld center $Z(\mathcal{C})$, and different UFCs $\mathcal{C}$ associated to the iMPO symmetries can give the same topological order if their centers are isomorphic [64]. To deal with this redundancy, we compute the center by constructing idempotents of the tube algebra and compute invariants such as the topological S and T matrices which encode mutual statistics and self-statistics of the emergent anyons. While the S and T matrices provide a useful characterization of the type of topological order, in general they do not uniquely specify the modular category $Z(\mathcal{C})$ [65]. By explicitly constructing $Z(\mathcal{C})$, our approach does not suffer from this problem.

The method we use has similarities with previous approaches where one looks for stringlike operators on the physical level that commute with the Hamiltonian called ribbon operators [66]. An important fact is that in these approaches, when moving away from the fixed point, these ribbon operators get dressed [67] and their width is proportional to the correlation length. In contrast, in our approach, the iMPO symmetries are not fattened when perturbing the system away from the fixed point since they act purely on the virtual level.

The paper is organized in Secs. II–IX where we gradually introduce subsequent elements of the algorithm. In Sec. II we give a brief review of $(2+1)$-dimensional $[(2+1)\mathrm{d}]$ topological order in PEPS and virtual MPO symmetries, the properties of which are governed by the F symbols of a UFC $\mathcal{C}$ that we aim to numerically determine for a generic iPEPS. In Sec. III we define fixed points of the iPEPS transfer matrix in the form of iMPS and introduce iMPO symmetries that map between different fixed points. We also identify fusion rules of the iMPO symmetries that are isomorphic with the fusion rules of some input category $\mathcal{C}$. In Sec. IV we introduce X zippers that are gauge transformations between products of two iMPO symmetries acting on a trivial fixed point of the transfer matrix and a single iMPO symmetry applied to the same trivial fixed point. We distinguish between up and down X zippers for, respectively, up and down fixed points. In Sec. V we introduce and construct more elementary Y zippers. Each Y zipper is a gauge transformation between a product of an iMPO symmetry and a fixed point of the transfer matrix and the resulting fixed point. X zippers can be constructed out of the elementary Y zippers. In Sec. VI pairs of complementary left and right X zippers are normalized to become pairs of gauge and inverse gauge transformations. In particular, a nontrivial normalization between up and down zippers is imposed. In Sec. VII we construct F symbols out of the normalized up and down X zippers. The fusion symbols have arbitrary/random numerical gauge. In Sec. VIII we parametrize the gauge freedom and outline how the F symbols can be brought to some canonical gauge that allows to identify the topological order. In Sec. IX we algebraically construct the gauge-invariant central idempotents of the tube algebra made of the zippers, which when inserted into iPEPS, as in Fig. 1, can be thought of as projectors onto minimally entangled states (MES). However, here we do not construct the MES but use the central idempotents of the tube algebra to directly extract topological S and T matrices [54,68]. Unlike the F symbols, the S and T matrices are gauge-invariant observables with a physical interpretation of statistics of the emergent anyons. In contrast to Refs. [49,52], here they are obtained by algebraic manipulation from the F symbols, the calculation of which is a purely 1D problem, which significantly reduces the complexity of the numerical algorithms. The route via F symbols therefore provides an alternative that is potentially more stable numerically. The paper is closed with a brief summary of the algorithm in Sec. X and an outlook towards future applications.

II. MPO SYMMETRIES IN PEPS

A necessary condition for a tensor network to exhibit topological order is the existence of stringlike operators on the virtual level that can be freely moved through the lattice. These operators are represented as MPO symmetries, that at the level of the local PEPS tensors satisfy the pulling-through

condition:

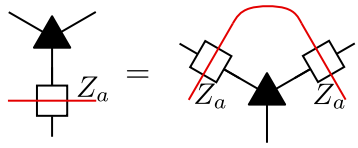

(1)

With periodic boundary conditions these MPO symmetries, which we denote as Z_a, form a representation of a fusion ring

$$Z_a Z_b = \sum_c N_{ab}^c Z_c, \tag{2}$$

where, for the remainder, we will restrict to the multiplicity-free case, i.e., $N_{ab}^c = 0, 1$. Locally this implies the existence of a fusion tensor X_{ab}^c that satisfies the zipper condition

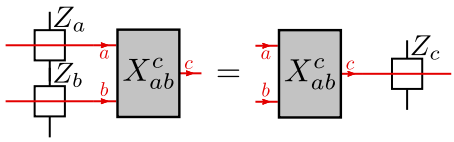

(3)

Multiplication of these MPO symmetries is associative, which imposes the following condition on the fusion tensors:

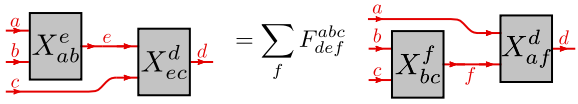

(4)

where $F_{def}^{abc} = (F_d^{abc})_e^f$ is a unitary matrix from e to f. These F symbols satisfy a consistency condition known as the pentagon equation:

$$\sum_f F_{def}^{abc} F_{hfj}^{bci} F_{gdh}^{afi} = F_{geh}^{abj} F_{gdj}^{eci}, \tag{5}$$

which turns the data N_{ab}^c and F_{def}^{abc} into consistent a unitary fusion category (UFC) $\mathcal{C}$. This UFC completely determines the topological order of the PEPS, and it is the goal of this work to numerically determine its data for an arbitrary PEPS tensor.

III. NUMERICAL MPO SYMMETRIES

The iPEPS representing the ground state on an infinite lattice $|\psi\rangle$ is assumed to be normalized: $\langle\psi|\psi\rangle = n$. Its norm, which is a contraction between the iPEPS (ket) and its complex conjugate (bra), is a 2D tensor network made of double iPEPS tensors shown in Fig. 2(a). Each row of the network is a horizontal transfer matrix Ω_h in Fig. 2(b). The transfer matrix has several leading up eigenvectors $|v_i^U)$ numbered by i, whose degenerate leading eigenvalue is 1 (hence the double iPEPS with n leading eigenvectors is normalized to n). These *boundary fixed points* can be reshaped as iMPO's, v_i^U, acting between virtual bra and ket indices. Together with their corresponding biorthonormal down eigenvectors $(v_i^D|$, that can be also reshaped as iMPO, v_i^D, they satisfy

$$\Omega_h \approx 1 \sum_{i=1}^{n} |v_i^U)(v_i^D|, \tag{6}$$

$$\delta_{ij} = (v_i^U|v_j^D) = \mathrm{Tr}\,(v_i^U)^T v_j^D. \tag{7}$$

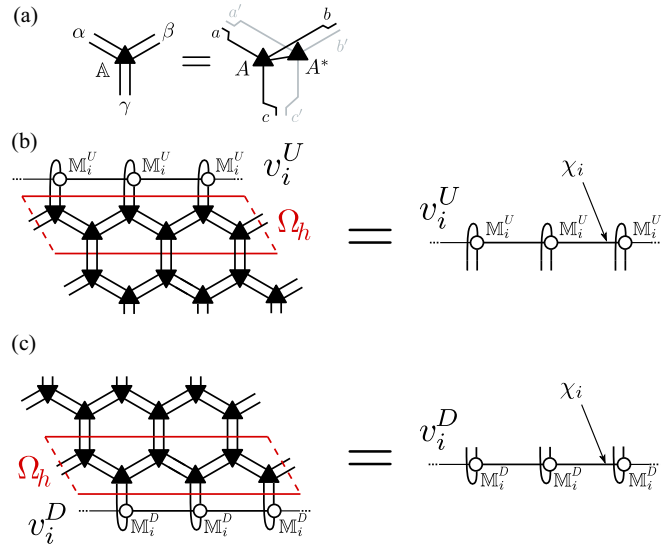

FIG. 2. Transfer matrix. In (a), graphical representation of a double iPEPS tensor $\mathbb{A}$ that is made out of an iPEPS tensor A contracted through a physical index with its complex conjugate A^*. In (b) and (c), a horizontal row of $\mathbb{A}$ makes a horizontal transfer matrix Ω_h. Its leading up eigenvectors $(v_i^U|$ and down eigenvectors, $(v_i^D|$, with the leading degenerate eigenvalue 1, can be obtained with the VUMPS algorithm [69,70]. The eigenvector can be reshaped into an iMPO form v_i^U. The uniform v_i^U is made of tensors $\mathbb{M}_i^U$ with bond dimension χ_i.

The first and the most important step to identify the topological order is finding the virtual iMPO symmetries of the iPEPS as their existence is a necessary condition for the iPEPS to exhibit topological order. As described in Refs. [49,52], the iMPO symmetries Z_a are found numerically as operators mapping between different iMPO boundary fixed points v_i:

$$v_i^U Z_a = \sum_k \delta_{iak} v_k^U,$$
$$v_i^D Z_a^T = \sum_k \bar{\delta}_{iak} v_k^D. \tag{8}$$

Here δ_{iak} and $\bar{\delta}_{iak}$ take values either 0 or 1 and in general they do not have to be the same. A trivial $v_1^{U,D}$ can be identified such that its trace with all the iMPO symmetries is equal 1: $\mathrm{Tr}(v_1^U Z_a v_1^D Z_a^\dagger) = 1$. In particular, for the up eigenvector v_1^U all other $v_{i>1}^U$ are obtained from it by the action of corresponding iMPO symmetries:

$$v_1^U Z_a = v_a^U, \tag{9}$$

while at the same time for the down eigenvectors

$$v_1^D Z_a^T = v_{\bar{a}}^D. \tag{10}$$

Each symmetry Z_a, including the trivial $Z_1 = \mathbb{I}$, represents certain anyon type a. Here $\bar{a}$ is an inverse of anyon type a that in general can be different than a. We note that these numerical iMPO symmetries defined in this way are only required to be symmetries of the iPEPS in the sense that they can be pushed through an entire row/column of the network, and in general will not satisfy the local pulling through condition of (1).

The iMPO symmetries can be obtained by variational minimization of a cost function that follows from Eqs. (9) and (10):

$$\left|v_1^U Z_a - v_a^U\right|^2 + \left|v_1^D Z_a^T - v_{\bar{a}}^D\right|^2. \tag{11}$$

Here Z_a is made of tensors z_a and v_a of $\mathbb{M}_a^U$. The cost function is quadratic in the infinite MPO symmetry Z_a but highly nonlinear in its tensor z_a. The minimization is performed with respect to z_a in a quasilocal manner. Namely, we choose one tensor z_a in the infinite Z_a and minimize with respect to it as if it were independent of all other tensors z_a. As the cost function is quadratic in the chosen tensor, its derivative with respect to $z_a^\dagger$ yields a linear equation for z_a. Its solution is a candidate to be substituted in place of all tensors z_a. In practice, we substitute its linear combination with the previous z_a with coefficients optimized to minimize the global cost function. This optimization is done in the same way as in Ref. [48]. This quasilocal procedure is iterated until convergence of the cost function. In order to avoid local minima, the whole minimization is repeated several times, with different random initial conditions.

In order to minimize the effect of the unnecessary modes in the null space of an iMPO symmetry acting on the up and down boundary eigenvectors the bond dimension of Z_a, χ_a, has to be the minimal one that still allows the cost function to be nullified. By definition, this cost function guarantees the correct action of the symmetries on the boundary fixed points but not the "abstract" fusion ring (2). However, the algebra is satisfied in a weaker sense:

$$v_i^U Z_a Z_b = \sum_c N_{ab}^c\, v_i^U Z_c, \tag{12}$$

$$v_i^D Z_a^T Z_b^T = \sum_d N_{ba}^d\, v_i^D Z_d^T, \tag{13}$$

i.e., when applied to any boundary fixed point. This is all that we need in the following construction.

Just as (2) is replaced by (12) and (13), in the realm of numerical iMPO symmetries, the definition of the F symbol is replaced by

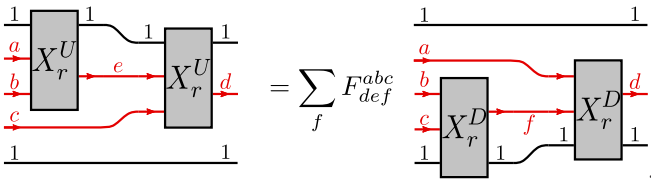

(14)

This diagram includes up and down boundary fixed points in order to execute the weaker "numerical" algebra (12) and (13). Accordingly, we introduce more general up and down zippers, X^U and X^D, that realize the fusions in (12) and (13). Their construction is the subject of Secs. IV, V, and VI.

Before proceeding to the X zippers in Sec. IV, we first illustrate this numerical procedure for iMPO symmetries in the following models. Some of the examples are the same as in Ref. [52] but notice that here the symmetries have to be recalculated because the cost function in (11) is in principle more demanding as it has two terms instead of just one. Indeed, in Refs. [49,52] it was enough for an iMPO symmetry to satisfy only one of conditions (9) and (10) because the iMPO symmetries were inserted in an iPEPS as in Fig. 1 and, therefore, it was enough that they acted properly on either the up or the down boundary of the iPEPS. In the present method we use them in the diagrammatic equation (14) where on the left-hand side they act on the up boundary and on the right-hand side on the down one. Therefore, for the equation to make sense, both their up and down action has to be correct.

Finally, as a last remark before we proceed to the examples, numerically there is a freedom of the global phase of the eigenvectors $v_i^{U,D}$, which can be partially eliminated (up to minus sign) by requiring their Hermiticity (when applicable). In general, the random global phases change the fusion rules, so that only their magnitudes are 0 or 1, $|N_{ab}^c| = 0, 1$. However, in all the examples below the random global phases are adjusted so that all N_{ab}^c are real, either 0 or 1.

A. Toric code and double semions

For analytic fixed-point tensors defined in Appendix A transfer matrix Ω_h has two numerical boundary fixed points $v_{1,2}^{U,D}$ and one nontrivial numerical iMPO symmetry Z_2 which fulfils the Z_2 algebra:

$$\left.\begin{aligned} v_1^U Z_2 &= v_2^U \\ v_2^U Z_2 &= v_1^U \end{aligned}\right\} \Rightarrow Z_2 Z_2 = \mathbb{I}. \tag{15}$$

The cost function (11) was minimized to zero within machine precision. The fusion rules can be summarized as

$$N_{11}^1 = N_{22}^1 = 1 \tag{16}$$

with all possible permutation of indices. It has to be strongly emphasized that in general the numerical Z_2 iMPO symmetry is not necessarily nullified outside the support subspace of the boundary eigenvectors, therefore, the ring on the right of (15) is valid only in the sense of the equalities on the left. The same reservation applies to all fusion rules to be identified numerically in the rest of this paper.

B. Kitaev model

As a realistic example of the toric code universality class we consider the Kitaev model on a honeycomb lattice defined by the following Hamiltonian:

$$\mathcal{H} = -\sum_{\alpha=x,y,z} J_\alpha \sum_{\alpha\ \text{links}} \sigma_i^\alpha \sigma_j^\alpha. \tag{17}$$

Here, σ_i^α, $\alpha = x, y, z$, are Pauli matrices acting on site i. We set $J_z = 1$ and study the model along the line $J = J_x = J_y \in (0, 0.5)$. The iPEPS ground state was obtained in Ref. [49] by variational optimization. For iPEPS bond dimension $D = 4$ we find that the bond dimension $\chi = 4$ of boundary iMPO's $v_{1,2}^{U,D}$ suffices to faithfully capture the entanglement properties of the phase. An accurate iMPO symmetry Z_2 is found with the minimal nontrivial bond dimension $\chi_Z = 2$. Its error can be quantified by two numbers:

$$\begin{aligned} \epsilon_Z^U &= \left|1 - \Lambda\left[\langle v_1^U Z_2 | v_2^U\rangle\right]\right|, \\ \epsilon_Z^D &= \left|1 - \Lambda\left[\langle v_1^D Z_2^T | v_2^D\rangle\right]\right|. \end{aligned} \tag{18}$$

Here $\Lambda(x)$ is the leading eigenvalue of a transfer matrix of overlap x. The errors are listed in the following Table I. Even

TABLE I. The errors (18) of the fusion ring of the numerical iMPO symmetry Z_2 with the corresponding up and down eigenvectors $v_1^{U,D}$. Here $J = J_x = J_y$ is the coupling constant in the Kitaev model with $J_z = 1$ (17). The iPEPS approximating its ground state with bond dimension $D = 4$ was obtained by variational optimization [49]. Here ξ is the correlation length calculated from the second leading eigenvalue of the iPEPS transfer matrix in the environment of the boundary eigenvectors.

J	ξ	ϵ_Z^U	ϵ_Z^D
0.4	0.21	$O(10^{-3})$	$O(10^{-3})$
0.42	0.22	$O(10^{-2})$	$O(10^{-2})$
0.44	0.23	$O(10^{-4})$	$O(10^{-4})$
0.46	0.25	$O(10^{-2})$	$O(10^{-2})$
0.48	0.26	$O(10^{-3})$	$O(10^{-3})$

though the numerical iPEPS tensors do not assume any symmetry or any special gauge, and their bond dimension is small, the iMPO symmetries turn out to be very accurate.

C. Twisted quantum double of $\mathbb{Z}_3$

For this example, the transfer matrix Ω_h has three boundary fixed points $v_{1,2,3}^{U,D}$, out of which only one, v_1^U and corresponding v_1^D, is Hermitian and it plays the role of the trivial boundary. The other two boundary fixed points are their own Hermitian conjugates: $v_2^{U,D} = (v_3^{U,D})^\dagger$. Here the labels in Eq. (11) are not self-inverse, i.e., $a \neq \bar{a}$ for $a = 2, 3$. The iMPO symmetry has bond dimension $\chi = 2$ and it fulfills

$$\left.\begin{aligned} v_1^U Z_q &= v_2^U,\ v_1^U Z_{q^*} = v_3^U \\ v_2^U Z_q &= v_3^U,\ v_2^U Z_{q^*} = v_1^U \\ v_3^U Z_q &= v_1^U,\ v_3^U Z_{q^*} = v_2^U \end{aligned}\right\} \Rightarrow Z_q Z_{q^*} = \mathbb{I}, \tag{19}$$

$$\left.\begin{aligned} v_1^D Z_q^T &= v_3^D,\ v_1^D Z_{q^*}^T = v_2^D \\ v_2^D Z_q^T &= v_1^D,\ v_2^D Z_{q^*}^T = v_3^D \\ v_3^D Z_q^T &= v_2^D,\ v_3^D Z_{q^*}^T = v_1^D \end{aligned}\right\} \Rightarrow Z_{q^*} Z_q = \mathbb{I}. \tag{20}$$

The two iMPO symmetries Z_q, Z_{q^*}, are denoted with the subscripts $q, q^* = e^{\pm 2i\pi/3}$. Despite different fusions with the eigenvectors $\delta_{iak} \neq \bar{\delta}_{iak}$ the fusion rules of the iMPO symmetries are given by the following nonzero elements of the fusion tensor:

$$\begin{aligned} \forall_{i=1,q,q^*}\ N_{1i}^i = N_{i1}^i = 1, \\ N_{qq^*}^1 = N_{q^*q}^1 = N_{qq}^{q^*} = N_{q^*q^*}^q = 1. \end{aligned} \tag{21}$$

In this case the anyon types q and q^* are the inverses of each other, which justifies the labeling.

D. Fibonacci string net

Here we employed the iPEPS tensors for a fixed point Fibonacci string-net model presented in Appendix A. The transfer matrix Ω_h has two numerical boundary fixed points $v_{1,2}^{U,D}$ and one nontrivial numerical iMPO symmetry Z_τ which fulfills

$$\left.\begin{aligned} v_1^U Z_\tau &= v_2^U \\ v_2^U Z_\tau &= v_1^U + v_2^U \end{aligned}\right\} \Rightarrow Z_\tau Z_\tau = \mathbb{I} + Z_\tau. \tag{22}$$

TABLE II. The errors (18) of the fusion ring of the the numerical iMPO symmetry with the corresponding up and down eigenvectors $v_1^{U,D}$. Parameter β represents the perturbation strength from Eq. (24), while ξ is the corresponding correlation length calculated from the second leading eigenvalue of the iPEPS transfer matrix in the environment of the boundary eigenvectors.

β	ξ	ϵ_Z^U	ϵ_Z^D
0.01	0.23	$O(10^{-7})$	$O(10^{-7})$
0.05	0.42	$O(10^{-4})$	$O(10^{-3})$
0.12	1.04	$O(10^{-4})$	$O(10^{-2})$
0.15	2.32	$O(10^{-2})$	0.05

Again, the cost function (11) was minimized to vanish up to machine precision and the fusion on the right holds only in the sense of the equalities on the left. The fusion algebra on the right of (22) allows us to label the iMPO symmetry with a non-Abelian Fibonacci anyon τ. The fusion rules can be summarized as

$$N_{11}^1 = N_{\tau\tau}^1 = N_{\tau\tau}^\tau = 1. \tag{23}$$

with all possible permutation of indices.

E. Fibonacci string net with local filtering

In order to drive the iPEPS away from a fixed point and introduce a finite correlation length, we apply the local filtering [71–73] to the fixed point of the Fibonacci string-net model. The modification has the following form:

$$|\Psi\rangle \rightarrow \prod_i e^{\beta\sigma_i^z} |\Psi\rangle, \tag{24}$$

where i runs over all physical indices, σ^z is the Pauli matrix, and β is a parameter. Correlation lengths ξ are listed in Table II. In the table we also present errors (18) of the two terms appearing in the cost function. The difference between errors of ϵ_Z^U, ϵ_Z^D arises from the fact that with growing correlation length it becomes harder to nullify both errors at the same time, therefore, in order to ensure convergence, in the step where we find an optimal update of tensor z_a we use only one of the conditions (18), namely, ϵ_Z^U.

F. Ising string net

Here again we employed the iPEPS tensors for a fixed-point Ising string-net model presented in Appendix A. This time, each transfer matrix has three numerical boundary fixed points, $v_{1,2,3}^{U,D}$, corresponding to three anyon types of the input category: $1, \sigma, \psi$. We found two nontrivial iMPO symmetries, labeled as Z_σ and Z_ψ. The fixed points and the symmetries are related by the following set of equations:

$$\left.\begin{aligned} v_1^U Z_\psi &= v_2^U \\ v_2^U Z_\psi &= v_1^U \\ v_3^U Z_\psi &= v_3^U \end{aligned}\right\} \Rightarrow Z_\psi Z_\psi = \mathbb{I}, \tag{25}$$

$$\left.\begin{aligned} v_1^U Z_\sigma &= v_3^U \\ v_2^U Z_\sigma &= v_3^U \\ v_3^U Z_\sigma &= v_1^U + v_2^U \end{aligned}\right\} \Rightarrow Z_\sigma Z_\sigma = \mathbb{I} + Z_\psi. \tag{26}$$

The cost function (11) was minimized to machine precision. Furthermore, we verified that with machine precision the symmetries satisfy

$$v_i^U Z_\sigma Z_\psi = v_i^U Z_\sigma \Rightarrow Z_\sigma Z_\psi = Z_\sigma. \tag{27}$$

The equations justify labeling of the symmetries. The fusion rules can be summarized as

$$N_{11}^1 = N_{\sigma\sigma}^1 = N_{\psi\psi}^1 = N_{\psi\psi}^\sigma = 1 \tag{28}$$

with all possible permutation of indices.

G. Quantum double of S_3 and Rep(S_3) string net

In this section we analyze two different iPEPS representations from Ref. [64] for the quantum double S_3 and the Rep(S_3) string-net model, with MPO symmetries, respectively, given by UFCs $\mathcal{C}_1 = \mathrm{Rep}(S_3)$ and $\mathcal{C}_2 = \mathrm{Vec}_{S_3}$. These two iPEPS representations describe the same topologically ordered phase since $Z[\mathrm{Rep}(S_3)] = Z(\mathrm{Vec}_{S_3})$.

1. *Rep(S_3) MPO symmetries*

In this representation iPEPS tensor has virtual bond dimension $D = 6$ and its related transfer matrix Ω_h has three leading eigenvectors $v_{1,2,3}^{U,D}$ corresponding to three anyon types $1, \pi, \psi$. There are two nontrivial iMPO symmetries, with corresponding labels π, ψ and they fulfill the following fusion rules with the eigenvectors:

$$\left.\begin{aligned} v_1^U Z_\psi &= v_3^U \\ v_2^U Z_\psi &= v_2^U + v_3^U \\ v_3^U Z_\psi &= v_1^U \end{aligned}\right\} \Rightarrow Z_\psi Z_\psi = \mathbb{I}, \tag{29}$$

$$\left.\begin{aligned} v_1^U Z_\pi &= v_3^U \\ v_2^U Z_\pi &= v_1^U + v_2^U + v_3^U \\ v_3^U Z_\pi &= v_1^U \end{aligned}\right\} \Rightarrow Z_\sigma Z_\sigma = \mathbb{I} + Z_\psi + Z_\pi. \tag{30}$$

The same set of equations can be written for the down eigenvectors. Moreover, we observe that

$$v_i^U Z_\pi Z_\psi = v_i^U Z_\pi \Rightarrow Z_\pi Z_\psi = Z_\pi, \tag{31}$$

which enables identification of all allowed fusion rules:

$$N_{11}^1 = N_{\pi\pi}^1 = N_{\psi\psi}^1 = N_{\psi\psi}^\sigma = N_{\pi\pi}^\pi = 1 \tag{32}$$

with all possible permutation of indices.

2. *Vec$_{S_3}$ MPO symmetries*

In this representation the iPEPS tensor has bond dimension that is just $D = 4$ while its related transfer matrix Ω_h has degeneracy 6 corresponding to six leading eigenvectors $v_{1,2,3,4,5,6}^{U,D}$. There are five nontrivial iMPO symmetries Z_a, which are all product iMPOs. There is only one eigenvector, which we label as identity, for which $\mathrm{Tr}(v_1^U Z_a v_1^D (Z_a)^\dagger) = 1$ for all $a = 1, \ldots, 6$. All the remaining up and down eigenvectors can be obtained from $v_1^{U,D}$ by proper action of the iMPO symmetries:

$$\begin{aligned} v_1^U Z_a &= v_a^U, \ \forall\, a = 1,2,3,4,5,6 \\ v_1^D Z_a^T &= v_a^D, \ \forall\, a = 1,2,3,4 \\ v_1^D Z_5^T &= v_6^D, \ v_1^D Z_6^T = v_5^D. \end{aligned} \tag{33}$$

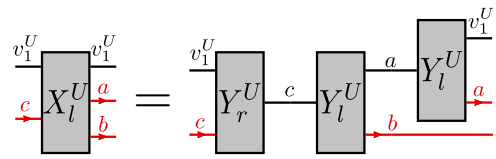

FIG. 3. Contraction of Y zippers that makes an X zipper. Here we show only U zippers but similar equations hold for their D counterparts. We distinguish between left l and right r zippers. Contraction of a left zipper with its corresponding right zipper yields an identity. One is a pseudoinverse of the other.

In this case the fusion ring is non-Abelian in the sense that $N_{ab}^c \neq N_{ba}^c$ and apart from trivial fusion rules $N_{1a}^a = N_{a1}^a = 1$, there are 25 nontrivial ones, all equal 1:

$$\begin{aligned} &N_{22}^1, N_{33}^1, N_{44}^1, N_{65}^1, N_{56}^1, N_{63}^2, N_{54}^2, N_{35}^2, N_{46}^2, \\ &N_{52}^3, N_{64}^3, N_{45}^3, N_{26}^3, N_{62}^4, N_{53}^4, N_{25}^4, N_{36}^4, \\ &N_{32}^5, N_{43}^5, N_{24}^5, N_{66}^5, N_{42}^6, N_{23}^6, N_{34}^6, N_{55}^6. \end{aligned} \tag{34}$$

From this we notice that iMPO symmetries Z_a for $a = 1, 2, 3, 4$ are self-inverse, while Z_5 is the inverse of Z_6.

IV. NUMERICAL *X* ZIPPERS

In this work we employ the fundamental theorem of MPS [60,61] according to which there exist an invertible gauge transformation G_l between two tensors A^i and B^i, where i is the "physical" index, both in a canonical form, generating equal iMPS's such that

$$A^i = G_l B^i G_r, \tag{35}$$

where $G_r = G_l^{-1}$. It can be further extended to iMPO and products of iMPO's where, e.g., $A = v_i Z_a$ and $B = v_k$. In that case the bond dimension of the product $v_i Z_a$ is usually bigger than the bond dimension of v_k: $\chi_i \chi_z > \chi_k$. Therefore, the gauge transformation G_l is actually a composition of an isometry U of dimensions $(\chi_i \chi_z, \chi_k)$ and an invertible $\chi_k \times \chi_k$ matrix g. G_r is a pseudoinverse of G_l and vice versa.

Due to the algebra of iMPO symmetries (2), which is fulfilled only when acting on the boundary fixed points (13), our goal is to find zipper tensors X_{ab}^c which serve as gauge transformations between products $v_1 Z_a Z_b$ and $v_1 Z_c$:

$$v_1 Z_a Z_b \overset{X_{ab}^c}{\longleftrightarrow} v_1 Z_c. \tag{36}$$

Here we consider only the trivial fixed point v_1 to make sure the fusions actually occur only between the iMPO symmetries Z.

This goal can be achieved in two steps, first by obtaining smaller zippers Y_{ia}^k which fuse a product $v_i Z_a$ into a single MPO v_k. The second step is the proper contraction of zippers Y_{ia}^k to form X_{ab}^c as shown in Fig. 3.

V. NUMERICAL *Y* ZIPPERS

The iMPO symmetry algebra Z_a includes a trivial symmetry $Z_1 = \mathbb{I}$ corresponding to the trivial anyon type. This identity iMPO is a product of identity matrices and has bond dimension $\chi_1 = 1$. Therefore, all the zippers $(Y_l)_{j1}^i$, together with their r (inverse) counterparts, are trivial identity matrices

of dimensions $\chi_j \times \chi_j$. We emphasize again that Z_1 as a product of identity matrices is sufficient for our construction because it still acts as the identity on the support subspace of PEPS, but it is not an exact MPO symmetry from Ref. [54], where a larger bond dimension is needed to encode the identity action on the relevant subspace only.

From now on we focus the attention on nontrivial zippers between the left- and right-hand sides of the equation $v_j Z_a = \sum_k \delta_{jak} v_k$ with $a > 1$. The product MPO tensor $M = v_j Z_a$ is either normal, for which a transfer matrix of $\mathrm{Tr} MM^\dagger$ has only one leading eigenvalue equal 1, or a direct sum of normal tensors, so the transfer matrix has several degenerate leading eigenvalues equal 1. In both cases we proceed by bringing the tensors M into left-canonical form using a repeated QR decomposition. For a fixed point of QR decomposition the relation between the initial tensor and the converged canonical form is

$$LM^i = M_L^i L, \tag{37}$$

which means that the transformation bringing the tensor M^i into its canonical form M_L^i is

$$LM^i \mathrm{pinv}(L) = M_L^i. \tag{38}$$

Here i denotes "physical" indices of tensor M. The pseudoinverse deals with singularity due to too large bond dimension of M: $\chi_j \chi_a > \sum_k \chi_k$.

In the next step we reduce the bond dimension for M_L^i and find the gauge transformation relating it with one of the v_k^i tensors. Towards this end we construct a mixed transfer matrix for $\mathrm{Tr} M_L v_k^\dagger$. Its left fixed point σ_L is an isometry of dimension $\chi_j \chi_a \times \chi_k$ truncating the left-canonized product M_L to v_k:

$$\sigma_L^T M_L^i \mathrm{pinv}\left(\sigma_L^T\right) = v_k^i. \tag{39}$$

Putting the isometry together with the gauge transformation L we can write

$$(Y_l)_{ja}^k (v_j Z_a)^i (Y_r)_{ja}^k = v_k^i, \tag{40}$$

where

$$(Y_l)_{ja}^k = \sigma_L^T L, \tag{41}$$

$$(Y_r)_{ja}^k = \mathrm{pinv}(L)\mathrm{pinv}\left(\sigma_L^T\right). \tag{42}$$

In diagrammatic form (40) is

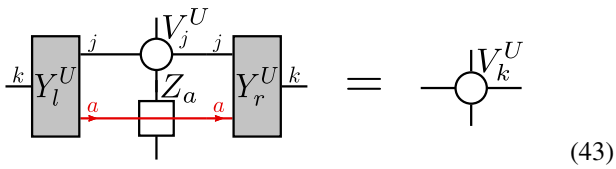

(43)

In all equations above we did not include the labels of the eigenvectors v_i, as there are two sets of them: v_i^U and v_i^D. However, the procedure is the same for both sets with a sole difference that for the down eigenvectors we need to use the transpose Z_a^T in place of Z_a.

VI. NORMALIZATION OF X ZIPPERS

Having the full set of required Y zippers $\{Y_l^U, Y_r^U, Y_l^D, Y_r^D\}$, we construct the X zippers according to Fig. 3. From this construction we get that

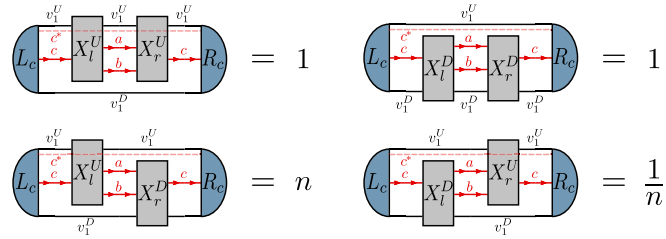

FIG. 4. Normalization conditions for the X_l and X_r zippers. The projectors $X_l^U X_r^U$ and $X_l^D X_r^D$ in the top row act like identities when inserted between the left L_c and right R_c fixed points of the transfer matrix $Tr(v_1^U \otimes Z_c \otimes v_1^D \otimes Z_c^\dagger)$. Here the $Z_c^\dagger$, which is necessary for the diagram to be nonzero is represented by the dashed line. The mixed products $X_l^U X_r^D$ and $X_l^D X_r^U$ in the bottom row yield n and $1/n$, respectively. The arbitrary n can be brought to 1 by rescaling the right X zippers.

$$\sum_{a,b} \left(X_l^U\right)_{ab}^c \left(X_r^U\right)_{ab}^c = \left(Y_r^U\right)_{1c}^c \left(Y_l^U\right)_{1c}^c, \tag{44}$$

which is not necessarily equal to identity matrix $\mathbb{I}_{\chi_1 \cdot \chi_c}$. However, it is a projector that acts like an identity when inserted between the left L_c and right R_c fixed points of the transfer matrix $Tr(v_1^U \otimes Z_c \otimes v_1^D \otimes Z_c^\dagger)$, as shown in the top row of Fig. 4 that includes also the complementary X^D case.

A similar normalization between X_l^U and its corresponding X_r^D is not automatic (see the bottom row of Fig. 4). Here the number n depends on somewhat arbitrary normalization of Y zippers making the X zippers. The number can be brought to 1 by rescaling, e.g., $X_l^D \to n X_l^D$ and $X_r^D \to (1/n) X_r^D$. Having thus properly normalized all of the X zippers we can proceed with the calculation of the F symbols.

VII. NUMERICAL F SYMBOLS

The last step of the algorithm is to calculate the F symbols in the equation in Eq. (14). This is a coupled set of equations for F_{def}^{abc} with different index f. In order to decouple them we project both sides onto $((X_l^D)_{ag}^d (X_l^D)_{bc}^g |$ from the left. At this point we verify that $((X_l^D)_{ag}^d (X_l^D)_{bc}^g | (X_r^D)_{bc}^g (X_r^D)_{ag}^d) = \delta_{gf}$ and we obtain an explicit formula

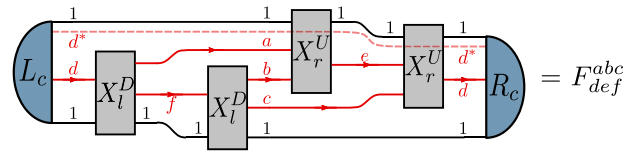

(45)

Here we have immersed the equation in the environment of left L_c and right R_c fixed points of the transfer matrix $Tr(v_1^U \otimes Z_d \otimes v_1^D \otimes Z_d^\dagger)$, the same as was used to find relative normalization of X^U and X^D zippers. The dotted red line denoted by d^* is the trace over indices corresponding to $Z_d^\dagger$.

A similar formula for an inverse of the matrix F is

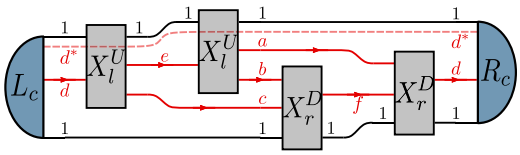

$$= F'^{abc}_{def} \tag{46}$$

Both F and F' satisfy the pentagon equation

$$\sum_f F^{abc}_{def} F^{bci}_{hfj} F^{afi}_{gdh} = F^{abj}_{geh} F^{eci}_{gdj}, \tag{47}$$

and describe the same topological order, although the value of their elements is in general different. The difference is manifestation of "gauge freedom" of F^{abc}_{def} due to remaining freedom in normalization of X zippers:

$$\left\{X_l^U, X_r^U, X_l^D, X_r^D\right\} \to \left\{\lambda X_l^U, \frac{1}{\lambda} X_r^U, \lambda X_l^D, \frac{1}{\lambda} X_r^D\right\}. \tag{48}$$

Here arbitrary $\lambda^c_{ab} \in \mathbb{C}$ depend on the labels of $X = X^c_{ab}$. Their values cannot be fixed by the Pentagon equation. λ^c_{ab} parametrize gauge freedom of the F symbols:

$$F^{abc}_{def} \to \frac{\lambda^f_{bc}\lambda^d_{af}}{\lambda^e_{ab}\lambda^d_{ec}} F^{abc}_{def}, \quad F'^{abc}_{def} \to \frac{\lambda^e_{ab}\lambda^d_{ec}}{\lambda^f_{bc}\lambda^d_{af}} F'^{abc}_{def}. \tag{49}$$

A straightforward way to proceed is to look for a gauge λ^c_{ab} that brings the F symbols, within numerical error, to a textbook form characteristic for a given type of topological order. This is what we do in the next section.

It is important to point out that the topological order is given by the monoidal center $Z(\mathcal{C})$, meaning that two fusion categories $\mathcal{C}_1$ and $\mathcal{C}_2$ that *a priori* look completely different may describe the same topological order [64], in which case $\mathcal{C}_1$ and $\mathcal{C}_2$ are said to be *Morita equivalent*. In order to deal with this redundancy, we compute the monoidal center in Sec. IX, as well as the corresponding S and T matrices.

VIII. F SYMBOLS IN CANONICAL GAUGE

We use the gauge freedom in (49) to bring F symbols to a canonical gauge where, for a unitary fusion category, the matrices F^{abc}_d are unitary and most elements of F are one, especially if any of a, b, c, d is trivial. To begin we notice that Eq. (49) implies that a product

$$F^{abc}_{def} F'^{abc}_{def} \tag{50}$$

is gauge invariant. Therefore, its square root will be used later to eliminate some of the gauge freedom of the F symbols.

Additionally, all X^c_{ab} where either $a = 1$ ($b = 1$) are chosen as identities between b and c (a and c). This choice fixes the gauge partially as $\lambda^c_{1c} = 1 = \lambda^c_{c1}$ but we are still left with freedom to choose the λ^c_{ab} where both $a \neq 1$ and $b \neq 1$. This residual gauge freedom leaves invariant all the F^{abc}_{def} where one of a, b, c is equal to 1.

Moreover, when there are only two anyon types in the input category, then also the F^{abc}_{1ef} are left invariant by the residual gauge transformation. The only F symbols that transform in a nontrivial way are

$$F^{222}_{212} \to \frac{\lambda^1_{22}}{\lambda^2_{22}\lambda^2_{22}} F^{222}_{212} \equiv \mu F^{222}_{212}, \tag{51}$$

$$F^{222}_{221} \to \frac{\lambda^2_{22}\lambda^2_{22}}{\lambda^1_{22}} F^{222}_{221} \equiv \frac{1}{\mu} F^{222}_{221}. \tag{52}$$

In the unitary gauge for every fixed set of indices a, b, c, d the matrix F^{abc}_{def} is unitary in indices ef. We can choose $|\mu|$ such that magnitudes of F^{222}_{2ef} become the same as square roots of corresponding products in (50). With a proper phase of μ the matrix F^{222}_{2ef} can be made unitary making manifest that the obtained F symbols describe unitary fusion category.

When there are more than two anyon types then there is a freedom

$$F^{abc}_{1ef} = F^{abc}_{1ca} \to \frac{\lambda^c_{ab}\lambda^1_{cc}}{\lambda^a_{bc}\lambda^1_{aa}} F^{abc}_{1ca}. \tag{53}$$

For $a = c$ this freedom is given by a simple ratio:

$$F^{aba}_{1aa} \to \frac{\lambda^a_{ab}}{\lambda^a_{ba}} F^{aba}_{1aa} \equiv \mu(a,b) F^{aba}_{1aa}, \tag{54}$$

which allows to determine first nontrivial gauge transformation and eliminate it from all F^{abc}_{def} in which it appears, by a substitution $\lambda^a_{ab} \to \mu(a,b)\lambda^a_{ba}$. The remaining scheme is largely model dependent, but the general idea is to replace unknown λ's with known ratios μ as we present on the examples below.

A. Toric code and double semions

We obtain the Y and X zipper tensors. For those two Abelian models there are two trivial Y zippers: $Y^1_{11}, Y^2_{21} = \mathbb{I}$ and two nontrivial Y zippers: Y^2_{12}, Y^1_{22} giving rise to four nonzero X zippers: $X^1_{11}, X^2_{12}, X^2_{21}, X^1_{22}$. For both the toric code and the double-semion model all gauges λ in Eq. (48) cancel each other in the expressions for F symbols. We obtain numerically exact F symbols immediately in the canonical gauge for toric code:

$$F^{abc}_{def} = N^e_{ab} N^e_{cd} N^f_{ad} N^f_{bc} \tag{55}$$

and the same for double semions with the exception for $F^{222}_{211} = -1$.

B. Kitaev model

We obtain the same set of Y and X zippers as for the toric code phase and then use them to find F symbols with an error calculated as the Frobenius norm:

$$\epsilon_F = ||F_{\text{numerical}} - F_{\text{canonical}}||. \tag{56}$$

Here $F_{\text{canonical}}$ are the exact F symbols in (55). Their errors are listed in Table III. Not quite surprisingly, good accuracy of the iMPO symmetry (see Table I) results in accurate F symbols.

C. Twisted quantum double of Z_3

We find three trivial Y zippers with both up and down eigenvectors Y^i_{i1} for $i = 1, q, q^*$ and six nontrivial with up

TABLE III. The error of the numerical F symbols, defined as the Frobenius norm of the difference with respect to the exact ones (56). Here $J = J_x = J_y$ is the coupling in the Kitaev Hamiltonian (17) with $J_z = 1$.

J	ϵ_F
0.40	$O(10^{-3})$
0.42	$O(10^{-3})$
0.44	$O(10^{-4})$
0.46	$O(10^{-2})$
0.48	$O(10^{-2})$

eigenvectors:

$$(Y^U)^2_{12}, (Y^U)^3_{13}, (Y^U)^1_{23}, (Y^U)^1_{32}, (Y^U)^3_{22}, (Y^U)^2_{33} \tag{57}$$

and with down eigenvectors

$$(Y^D)^3_{12}, (Y^D)^2_{13}, (Y^D)^3_{23}, (Y^D)^2_{32}, (Y^D)^1_{22}, (Y^D)^1_{33}, \tag{58}$$

which altogether give rise to a unique set of X zippers: trivial X^a_{1a}, X^a_{a1} for $a = 1, q, q^*$ and $X^3_{22}, X^2_{33}, X^1_{23}, X^1_{32}$. Therefore, there are four random residual gauges: $\lambda^1_{23}, \lambda^1_{32}, \lambda^3_{22}, \lambda^2_{33}$, which appear in only two combinations:

$$\rho_1 = \frac{\lambda^1_{23}}{\lambda^1_{32}}, \ \rho_2 = \frac{\lambda^1_{32}}{\lambda^3_{22}\lambda^2_{33}}, \tag{59}$$

where ρ_1 and its inverse fully fixes $F^{222}_{133}, F^{323}_{311}, F^{232}_{211}, F^{333}_{122}$ while ρ_2 fully fixes $F^{332}_{321}, F^{322}_{213}$ and there are only two remaining F symbols:

$$\begin{aligned} F^{223}_{231} &\to \rho_1\rho_2 F^{223}_{231}, \\ F^{233}_{312} &\to \frac{1}{\rho_1\rho_2} F^{233}_{312}. \end{aligned} \tag{60}$$

This procedure allows us to obtain $F^{abc}_{def} = N^e_{ab}N^e_{cd}N^f_{ad}N^f_{bc}$ with the exception of

$$F^{222}_{133} = F^{333}_{122} = \left(F^{332}_{321}\right)^* = \left(F^{223}_{231}\right)^* = e^{\frac{2i\pi}{3}}. \tag{61}$$

The obtained F symbols necessarily satisfy the pentagon equation, both before and after the gauge transformation. This is the only example we present, in which the F symbols and their inverses F^{-1} are not equal, but actually $(F^{abc}_{def})^{-1} = (F^{abc}_{def})^*$.

D. Fibonacci string net

We obtain two trivial Y zippers: $Y^1_{11}, Y^2_{21} = \mathbb{I}$ and three nontrivial Y zippers: $Y^2_{12}, Y^1_{22}, Y^2_{22}$ giving rise to five nonzero X zippers: $X^1_{11}, X^2_{12}, X^2_{21}, X^1_{22}, X^2_{22}$. With X zippers we obtain F symbols that satisfy the pentagon equation within machine precision. However, the obtained F symbols turn out to be in a random nonunitary gauge.

As the double Fibonacci model has two anyon types, the residual gauge freedom in Eq. (52) can be employed to adjust both F^{abc}_{def} or F'^{abc}_{def} to the absolute values obtained from a square root of the product (50) and then to fix their phase in such a way that F^{abc}_{def} and F'^{abc}_{def} become unitary in indices e, f within numerical precision. This way we obtain $F^{abc}_{def} = N^e_{ab}N^e_{cd}N^f_{ad}N^f_{bc}$ except for

$$F^{\tau\tau\tau}_{\tau 11} = -F^{\tau\tau\tau}_{\tau\tau\tau} = \frac{1}{d_\tau}, \ F^{\tau\tau\tau}_{\tau\tau 1} = F^{\tau\tau\tau}_{\tau 1\tau} = \frac{1}{\sqrt{d_\tau}}. \tag{62}$$

Here the quantum dimension $d_\tau = (\sqrt{5}+1)/2$.

TABLE IV. The error (56) of numerical F symbols. Here the first column represents the perturbation strength β.

β	ξ	ϵ_F
0.01	0.23	$O(10^{-7})$
0.05	0.42	$O(10^{-5})$
0.12	1.04	$O(10^{-2})$
0.15	2.32	$O(10^{-2})$

E. Fibonacci string net with local filtering

We applied the same algorithm for the local filtering that introduces a finite correlation length ξ and drives the state away from the fixed point. Errors of the obtained F symbols are listed in Table IV. The error remains small up to the correlation length $\xi = 2.32$. Better results for longer correlations lengths would require further improvement of the algorithm to obtain iMPO symmetries. We leave this refinement for future work.

F. Ising string net

As the double Ising model has three anyon types in the input category $\mathcal{C}$, there are five random residual gauges: $\lambda^1_{\psi\psi}, \lambda^1_{\sigma\sigma}, \lambda^\sigma_{\psi\sigma}, \lambda^\sigma_{\sigma\psi}, \lambda^\psi_{\sigma\sigma}$. They appear in only three combinations:

$$\rho_1 = \frac{\lambda^\sigma_{\psi\sigma}}{\lambda^\sigma_{\sigma\psi}}, \ \rho_2 = \frac{\lambda^1_{\sigma\sigma}}{\lambda^\sigma_{\sigma\psi}\lambda^\psi_{\sigma\sigma}}, \ \rho_3 = \frac{\lambda^1_{\psi\psi}}{\left(\lambda^\sigma_{\sigma\psi}\right)^2}. \tag{63}$$

Starting with ρ_1, which fully fixes $F^{\sigma\psi\sigma}_{1\sigma\sigma}$, $F^{\sigma\psi\sigma}_{\psi\sigma\sigma}$, and $F^{\sigma\sigma\sigma}_{\sigma\psi\psi}$, we find ρ_2 fixing $F^{\sigma\sigma\psi}_{\psi 1\sigma}$, $F^{\sigma\sigma\sigma}_{\sigma 1\psi}$, and finally ρ_3 which is fully fixing $F^{\sigma\psi\psi}_{\sigma\sigma 1}$. The remaining F symbols are fixed by proper combinations:

$$\begin{aligned} F^{\psi\psi\sigma}_{\sigma 1\sigma} &\to \frac{\rho_3}{\rho_1^2} F^{\psi\psi\sigma}_{\sigma 1\sigma}, \\ F^{\psi\sigma\sigma}_{1\sigma\psi} &\to \frac{\rho_1\rho_2}{\rho_3} F^{\psi\sigma\sigma}_{1\sigma\psi}, \\ F^{\psi\sigma\sigma}_{\psi\sigma 1} &\to \frac{\rho_1}{\rho_2} F^{\psi\sigma\sigma}_{\psi\sigma 1}, \\ F^{\sigma\sigma\sigma}_{\sigma\psi 1} &\to \frac{\rho_1}{\rho_2} F^{\sigma\sigma\sigma}_{\sigma\psi 1}, \\ F^{\sigma\sigma\psi}_{1\psi\sigma} &\to \frac{\rho_3}{\rho_2} F^{\sigma\sigma\psi}_{1\psi\sigma}. \end{aligned} \tag{64}$$

This way we obtain $F^{abc}_{def} = N^e_{ab}N^e_{cd}N^f_{ad}N^f_{bc}$ except for

$$F^{\sigma\sigma\sigma}_{\sigma 11} = F^{\sigma\sigma\sigma}_{\sigma 1\psi} = F^{\sigma\sigma\sigma}_{\sigma\psi 1} = -F^{\sigma\sigma\sigma}_{\sigma\psi\psi} = \frac{1}{\sqrt{2}}, \tag{65}$$

$$F^{\psi\sigma\psi}_{\sigma\sigma\sigma} = F^{\sigma\psi\sigma}_{\psi\sigma\sigma} = -1, \tag{66}$$

all with numerical precision.

G. Quantum double of S_3

1. Rep(S_3) MPO symmetries

Apart from the trivial X zippers with an identity symmetry $X^a_{1a} = X^a_{a1} = \mathbb{I}_a$ there are six nontrivial ones $X^1_{22}, X^1_{33}, X^2_{22}, X^3_{22}, X^2_{32}, X^2_{23}$, all with its corresponding gauge freedom λ^c_{ab}. However, there are only four independent variables:

$$\rho_1 = \frac{\lambda^2_{23}}{\lambda^2_{32}},\ \rho_2 = \frac{\left(\lambda^2_{22}\right)^2}{\lambda^1_{22}},\ \rho_3 = \frac{\lambda^1_{22}}{\lambda^3_{22}\lambda^1_{33}},\ \rho_4 = \frac{\lambda^1_{33}}{\left(\lambda^3_{22}\right)^2}. \quad (67)$$

After elimination of the gauge freedom from all possible F symbols containing the aforementioned ratios we obtain that $F^{abc}_{def} = N^e_{ab}N^e_{cd}N^f_{ad}N^f_{bc}$, except for

$$\begin{aligned} F^{322}_{222} = F^{232}_{222} = F^{223}_{222} = F^{222}_{322} = -1, \\ F^{222}_{211} = F^{222}_{231} = F^{222}_{213} = F^{222}_{223} = \tfrac{1}{d_\pi}, \\ F^{222}_{221} = F^{222}_{212} = -F^{222}_{232} = -F^{222}_{223} = \tfrac{1}{\sqrt{d_\pi}}, \\ F^{222}_{222} = 0, \end{aligned} \quad (68)$$

where $d_\pi = 2$ is the quantum dimension of π and the remaining quantum dimensions are $d_1 = d_\psi = 1$.

2. Vec(S_3) MPO symmetries

There are 25 nontrivial fusion rules N^c_{ab} giving rise to corresponding X zippers X^c_{ab}, hence, 25 random gauges λ^c_{ab}, which can be eliminated using only 20 ratios ρ_i. It can be done by subsequent substitution of certain ratios $\rho_i = \frac{\lambda^e_{ab}\lambda^d_{ec}}{\lambda^f_{bc}\lambda^d_{af}}$, so that the final F symbols are all trivial: $F^{abc}_{def} = N^e_{ab}N^e_{cd}N^f_{ad}N^f_{bc}$, with every index taking up to six values. All the quantum dimensions are $d_a = 1$.

At first glance the F symbols in both examples above may seem to describe completely different topological orders as they describe different unitary fusion categories UFC. However, the calculation of the Drinfeld center in the following sections proves that this is not the case.

IX. S AND T MATRICES FROM F SYMBOLS

The topological S and T matrices are gauge-invariant quantities, which in principle could be obtained from the F symbols in arbitrary gauge by considering proper gauge-canceling factors [74]. Here instead, we make use of the F symbols in canonical gauge, obtained in Sec. VIII, to derive a simpler expression.

An important observation is that the labels of all nonzero elements of both X and Y zippers define the possible fusions N^c_{ab} of the anyons in the category, from which we obtain their quantum dimensions d_a, as the largest magnitude eigenvalue of the N_a matrix. In this sense, fusion rules and quantum dimensions are exact independently of the correlations in the models.

In order to obtain all the anyons or definite anyonic sectors (MES) in the tensor network ansatz we need to find central idempotents of the algebra generated by elements $A_{abcd} \propto N^b_{da}N^b_{cd} \propto (X_r)^b_{da}(X_l)^b_{cd}$ (connected through the index b, but not summed over b), where we omit possible multiplicities as they are all equal 1 in our examples. Central idempotents, when inserted into PEPS, can be thought of as projectors onto states with well-defined anyon flux along the torus. The multiplication of the basis elements $e_i := A_{abcd}$ defines some algebra, from which we find both central and simple idempotents as described in Appendix B. The algebra of A_{abcd} can be used to calculate the action of the Dehn twist on a state with a symmetry Z_a along the torus [68]:

$$\begin{aligned} \tilde{T}(A_{abad}) &= A_{a1a\bar{a}}A_{abad} \\ &= \sum_{e,c}\sqrt{\frac{d_a d_{\bar{a}} d_c d_d}{d_e d_b}}\left(F^{\bar{a}ad}_{d1b}\right)^{-1}F^{\bar{a}da}_{deb}F^{a\bar{a}d}_{d1e}A_{acae}\delta_{cd}, \\ e_i &= \sum_j \tilde{T}_{ij}e_j. \end{aligned} \quad (69)$$

This formula gives rise to the $\tilde{T}$ matrix in the basis of $e_i \equiv A_{abcd}$. In the eigenbasis (the MES basis) this matrix is diagonal and contains the phases corresponding to topological spins: $T = \mathrm{diag}(\theta_1, \ldots, \theta_N)$. However, at this point we do not possess enough knowledge to assign anyon labels to them and certain topological spins belonging to multidimensional particles in non-Abelian anyon models are repeated (e.g., $\theta_{\tau\bar{\tau}}$ in the double Fibonacci string net and $\theta_{\sigma\bar{\sigma}}$ in the double Ising string net). Therefore, we proceed with the calculation of the topological S and T matrices in the MES basis. If we denote central idempotents inserted in PEPS to create a minimally entangled state in y direction by $\mathcal{P}^y_i$ and similarly in the x direction by $\mathcal{P}^x_i$, then the transformation between these two bases is actually an S matrix:

$$\mathcal{P}^y_i = \sum_j S_{ij}\mathcal{P}^x_j. \quad (70)$$

We can further write this expression in terms of the basis elements $e_k := A_{abcd}$:

$$\mathcal{P}^y_i = \sum_a c^i_a e^y_a = \sum_j S_{ij}\sum_b c^j_b e^x_b, \quad (71)$$

which written in the matrix forms without summations, with $E^{x,y}$ being the basis in x and y, respectively, B the basis change between x and y, P the matrix of coefficients of the central idempotents in the E basis, is

$$PE^y = PBE^x = SPE^x \Rightarrow S = PBP^{-1}. \quad (72)$$

Similarly we obtain the expression for the T matrix in the MES basis:

$$T = P\tilde{T}P^{-1}. \quad (73)$$

The $\tilde{T}$ is given in Eq. (69) and the basis change B is given by the combination of F symbols, as shown in [68]

$$S(A_{abad}) = \sum_e d_a\sqrt{\frac{d_d d_{\bar{d}}}{d_e d_b}}\left(F^{ad\bar{d}}_{ab1}\right)^* F^{d\bar{d}a}_{a1e}F^{da\bar{d}}_{abe}A_{\bar{d}e\bar{d}a}. \quad (74)$$

For non-Abelian anyon models, the inversion P^{-1} for two- or more-dimensional idempotents actually means the sum of inverted simple idempotents. Unlike the matrix of central idempotent, the matrix of simple idempotents P_{simple} in most cases is square and invertible. Technically, it means that the

matrix P_{simple} is made of rows of all simple idempotents, which makes it block diagonal with two (or more) rows in different blocks corresponding to the same anyon type. Next, we invert the matrix of simple idempotents P_{simple}, so that the columns of P^{-1}_{simple} correspond to the inverses of simple idempotents. In the end we sum up the columns that correspond to the same anyon flux to get P^{-1}. Moreover, the rows of P corresponding to anyon types that are supported on these multidimensional spaces have to be normalized (divided by their dimensionality).

A. Toric code, double semion, Fibonacci, and Ising string net

For all the RG fixed-point wave functions of toric code, double semion, double Fibonacci, and double Ising we obtain correct topological S and T matrices within machine precision. All the results are listed below.

(i) Toric code:

$$S_{\text{TC}} = \frac{1}{2}\begin{pmatrix} 1 & 1 & 1 & 1 \\ 1 & 1 & -1 & -1 \\ 1 & -1 & 1 & -1 \\ 1 & -1 & -1 & 1 \end{pmatrix},$$

$$T_{\text{TC}} = \begin{pmatrix} 1 & 0 & 0 & 0 \\ 0 & 1 & 0 & 0 \\ 0 & 0 & 1 & 0 \\ 0 & 0 & 0 & -1 \end{pmatrix}.$$

(ii) Double semion:

$$S_{\text{ds}} = \frac{1}{2}\begin{pmatrix} 1 & 1 \\ 1 & -1 \end{pmatrix}^{\otimes 2}, \qquad T_{\text{ds}} = \begin{pmatrix} 1 & 0 \\ 0 & i \end{pmatrix} \otimes \begin{pmatrix} 1 & 0 \\ 0 & -i \end{pmatrix}.$$

(iii) Double Fibonacci, with $\varphi = \frac{1+\sqrt{2}}{2}$:

$$S_{\text{dFib}} = \frac{1}{\varphi+2}\begin{pmatrix} 1 & \varphi \\ \varphi & -1 \end{pmatrix}^{\otimes 2},$$

$$T_{\text{dFib}} = \begin{pmatrix} 1 & 0 \\ 0 & e^{\frac{4i\pi}{5}} \end{pmatrix} \otimes \begin{pmatrix} 1 & 0 \\ 0 & e^{\frac{-4i\pi}{5}} \end{pmatrix}.$$

(iv) Double Ising:

$$S_{\text{dIs}} = \frac{1}{4}\begin{pmatrix} 1 & \sqrt{2} & 1 \\ \sqrt{2} & 0 & -\sqrt{2} \\ 1 & -\sqrt{2} & 1 \end{pmatrix}^{\otimes 2},$$

$$T_{\text{dIs}} = \begin{pmatrix} 1 & 0 & 0 \\ 0 & e^{\frac{i\pi}{8}} & 0 \\ 0 & 0 & -1 \end{pmatrix} \otimes \begin{pmatrix} 1 & 0 & 0 \\ 0 & e^{\frac{-i\pi}{8}} & 0 \\ 0 & 0 & -1 \end{pmatrix}.$$

B. Kitaev model

With the F symbols whose errors are listed in Table III we can recover topological S and T matrices. The same matrices were obtained in Ref. [49] by a different method. Interestingly, for $J = 0.44$ where the errors of the iMPO symmetries happen to be the most accurate (see Table I) the topological matrices obtained here are one order of magnitude more accurate (see Table V) than those in Ref. [49].

TABLE V. Maximal errors of the elements of the topological S and T matrices in the Kitaev model (17). Here $J = J_x = J_y$ for a fixed $J_z = 1$.

J	ϵ_S	ϵ_T
0.40	$O(10^{-3})$	$O(10^{-3})$
0.42	$O(10^{-4})$	$O(10^{-3})$
0.44	$O(10^{-4})$	$O(10^{-4})$
0.46	$O(10^{-3})$	$O(10^{-3})$
0.48	$O(10^{-3})$	$O(10^{-2})$

C. Fibonacci string net with local filtering

By direct application of the described procedure for perturbations $\beta = 0.01,\ 0.05$ we can recover topological modular matrices with satisfying precision as shown in the Table VI. For higher β in order to obtain the S_{Fib} and T_{Fib} matrices we need to improve the quality of F^{abc}_{def} to satisfy the pentagon equation (47) with better accuracy. Here we perform a simple Monte Carlo (MC), where we sweep over all nonzero elements of F tensor, apart from F^{111}_{111}, F^{211}_{221}, F^{121}_{222}, F^{112}_{212}, which are all equal 1 by construction. In a single MC move we change an element of F tensor $F'^{abc}_{def} = F^{abc}_{def} + \delta r_1$, where r_1 is a random complex number and $\delta = 0.01\epsilon(F)$ is the MC step with $\epsilon(F)$ being the error of the pentagon equation. We calculate the new error of the pentagon equation $\epsilon(F')$ and accept it if $\epsilon(F') < \epsilon(F)$ or check if the ratio $\frac{\epsilon(F)}{\epsilon(F')}$ is smaller than another random real number r_2 and accept the move if this is fulfilled. We perform such sweeps over all aforementioned elements of F tensor, which enables to obtain an error low enough to calculate the topological S and T matrices. We list the new error of F symbols together with the errors for the topological S and T matrices in Table VI. For $\beta = 0.15$, where the correlation length is $\xi = 2.32$, we can make a comparison with Ref. [52] and we see that the error of topological S matrix is of the same order while the error of topological T matrix is an order of magnitude bigger though the latter one is still negligible.

TABLE VI. The error of the final S and T matrices, ϵ_S and ϵ_T, respectively, calculated as the Frobenius norm of the difference between the numerical and the exact ones for different perturbation strengths β. Here χ is the bond dimension of the boundary eigenvectors $v_i^{U,D}$ used for the calculations. The numerical S and T matrices for bigger perturbations $\beta = 0.12, 0.15$ can be obtained only after the error of the numerical F symbols is reduced up to the value of ϵ_F^{MC} by simple Monte Carlo minimization of the error of pentagon equation.

β	ξ	χ	ϵ_S	ϵ_T	ϵ_F^{MC}
0.01	0.23	8	$O(10^{-7})$	$O(10^{-7})$	
0.05	0.42	12	$O(10^{-5})$	$O(10^{-5})$	
0.12	1.04	16	$O(10^{-3})$	$O(10^{-6})$	$O(10^{-3})$
0.15	2.32	20	$O(10^{-3})$	$O(10^{-6})$	$O(10^{-3})$

D. Twisted quantum double of $\mathbb{Z}_3$

For the twisted quantum double of $\mathbb{Z}_3$ we obtain the following T and S matrices:

$$\mathrm{diag}(T_{\mathbb{Z}_3}) = \left(1, 1, 1, e^{\frac{4i\pi}{9}}, e^{\frac{-8i\pi}{9}}, e^{\frac{-2i\pi}{9}}, e^{\frac{-2i\pi}{9}}, e^{\frac{-8i\pi}{9}}, e^{\frac{4i\pi}{9}}\right),$$

$$\frac{\arg(S_{\mathbb{Z}_3})}{2\pi} = \begin{pmatrix} 0 & 0 & 0 & 0 & 0 & 0 & 0 & 0 & 0 \\ 0 & 0 & 0 & -\frac{1}{3} & -\frac{1}{3} & -\frac{1}{3} & \frac{1}{3} & \frac{1}{3} & \frac{1}{3} \\ 0 & 0 & 0 & \frac{1}{3} & \frac{1}{3} & \frac{1}{3} & -\frac{1}{3} & -\frac{1}{3} & -\frac{1}{3} \\ 0 & -\frac{1}{3} & \frac{1}{3} & -\frac{4}{9} & \frac{2}{9} & -\frac{1}{9} & \frac{1}{9} & -\frac{2}{9} & \frac{4}{9} \\ 0 & -\frac{1}{3} & \frac{1}{3} & \frac{2}{9} & -\frac{1}{9} & -\frac{4}{9} & \frac{4}{9} & \frac{1}{9} & -\frac{2}{9} \\ 0 & -\frac{1}{3} & \frac{1}{3} & -\frac{1}{9} & -\frac{4}{9} & \frac{2}{9} & -\frac{2}{9} & \frac{4}{9} & \frac{1}{9} \\ 0 & \frac{1}{3} & -\frac{1}{3} & \frac{1}{9} & \frac{4}{9} & -\frac{2}{9} & \frac{2}{9} & -\frac{4}{9} & -\frac{1}{9} \\ 0 & \frac{1}{3} & -\frac{1}{3} & -\frac{2}{9} & \frac{1}{9} & \frac{4}{9} & -\frac{4}{9} & -\frac{1}{9} & \frac{2}{9} \\ 0 & \frac{1}{3} & -\frac{1}{3} & \frac{4}{9} & -\frac{2}{9} & \frac{1}{9} & -\frac{1}{9} & \frac{2}{9} & -\frac{4}{9} \end{pmatrix},$$

$$|(S_{\mathbb{Z}_3})_{ij}| = \frac{1}{3}.$$

E. Quantum double of S_3

For both iPEPS representations we obtain the topological S and T matrices which agree with machine precision with the exact ones up to the simultaneous permutation of columns and rows:

$$\mathrm{diag}(T_{S_3}) = \left(1, e^{\frac{-2i\cdot\pi}{3}}, 1, -1, e^{\frac{2i\cdot\pi}{3}}, 1, 1, 1\right),$$

$$S_{S_3} = \frac{1}{6}\begin{pmatrix} 1 & 3 & 2 & 1 & 2 & 3 & 2 & 2 \\ 3 & 3 & 0 & -3 & 0 & -3 & 0 & 0 \\ 2 & 0 & 4 & 2 & -2 & 0 & -2 & -2 \\ 1 & -3 & 2 & 1 & 2 & -3 & 2 & 2 \\ 2 & 0 & -2 & 2 & -2 & 0 & -2 & 4 \\ 3 & -3 & 0 & -3 & 0 & 3 & 0 & 0 \\ 2 & 0 & -2 & 2 & -2 & 0 & 4 & -2 \\ 2 & 0 & -2 & 2 & 4 & 0 & -2 & -2 \end{pmatrix}.$$

The algorithm we present in Appendix B fails to decompose the two-dimensional central idempotent corresponding to the anyon flux $(1, \pi)$ into simple idempotents, which should be done as shown in [68]:

$$(1, \pi) = (1, \pi)_{00} + (1, \pi)_{11},$$

$$(1, \pi) = \frac{1}{3}(2A_{1111} - A_{1515} - A_{1616}), \tag{75}$$

$$(1, \pi)_{00} = \frac{1}{3}\left(A_{1111} + e^{\frac{-2i\cdot\pi}{3}}A_{1515} + e^{\frac{2i\cdot\pi}{3}}A_{1616}\right), \tag{76}$$

$$(1, \pi)_{11} = \frac{1}{3}\left(A_{1111} + e^{\frac{2i\cdot\pi}{3}}A_{1515} + e^{\frac{-2i\cdot\pi}{3}}A_{1616}\right). \tag{77}$$

However, that is a necessary step to do in order to obtain correct modular S and T matrices shown above.

X. CONCLUSION AND OUTLOOK

The numerical method to obtain the F symbols of the fusion category fully characterizing the topological order can be summarized in the following few steps:

(i) Finding all boundary fixed points, both up and down, v_i^U, v_i^D of the double iPEPS horizontal transfer matrix Ω_h.

(ii) Calculating all iMPO symmetries Z_a mapping between different boundary fixed points: $v_i^U Z_a = v_j^u$ and $v_j^D Z_a^T = v_j^D$.

(iii) Finding the gauge transformations Y_{ia}^k between equal iMPOs $M = v_i Z_a$ and v_k for both up and down eigenvectors and combining them to yield zippers X_{ab}^c fusing the product of iMPO symmetries $v_1 Z_a Z_b$ into single iMPO symmetry $v_1 Z_c$.

(iv) Calculating the F symbols using the associativity of the fusions of iMPO symmetries Z_a.

(v) The numerical F symbols in the random gauge can be brought into canonical gauge by proper inspection of the freedom in the normalization of X_{ab}^c zippers. They can also be used to calculate gauge-invariant topological data in the form of S and T matrices encoding mutual and self statistics of the emergent anyons of the doubled category.

After slight purification of the F symbols, by minimizing the error of the pentagon equation, the method proved to give accurate results for states with correlation length up to $\xi = 2.3$. Their accuracy is comparable with those from Refs. [49,52]. On the other hand, in the realistic case of the numerically optimized iPEPS representing the ground state of the Kitaev model, we were able to obtain topological S and T matrices with accuracy an order of magnitude better than with the previous method [49]. A possible explanation is that the present method consists of significantly less numerical steps, therefore, it leaves less room for the accumulation of errors. Apart from the first step of finding the boundary fixed points, all the remaining steps are based on contractions of one-dimensional tensor networks. Finally, it provides not only topological S and T matrices, but also F symbols that allow for an unambiguous identification of topological order.

As mentioned in the Introduction, by studying the virtual iMPO symmetries rather than the physical Wilson line operators, we avoid the complications that arise due to the broadening of these Wilson lines away from the fixed point. Although we have shown that the method is applicable with nonzero correlation length, the correlation lengths for which the correct results are recovered are still rather small and it is clear there is still much room for improvement in several aspects of the algorithm.

Such improvements would allow us to study the change in topological order when driving a certain state through a phase transition. These phase transitions are characterized by the breaking and emergence of MPO symmetries, which should be reflected in the fixed-point structure. This becomes particularly interesting when considering variationally optimized iPEPS, where a specific choice of PEPS representation and corresponding MPO symmetries is not imposed but rather chosen by the algorithm. Close to a phase transition, we expect the algorithm to prefer the PEPS representation that most naturally allows the relevant MPO symmetries to be broken or emerge.

ACKNOWLEDGMENTS

Numerical calculations were performed in MATLAB with the help of `ncon` function [75] for tensor contractions. A.F. acknowledges financial support by Polish Ministry of Science and Education, Project No. DI2015 021345, from the budget funds for science under the Diamond Grant program. This research was also supported by Narodowe Centrum Nauki (NCN) under Grant No. 2019/35/B/ST3/01028 (A.F., J.D.) and Etiuda Grant No. 2020/36/T/ST3/00451 (A.F.). This work has received funding from the European Research Council (ERC) under the European Union's Horizon 2020 research and innovation programme (Grant Agreement No. 647905 (QUTE)). L.L. is supported by a Ph.D. fellowship from the Research Foundation Flanders (FWO).

APPENDIX A: iPEPS TENSORS

iPEPS tensors, shown in Fig. 5, are given by the following combination of F symbols and quantum dimensions d_i:

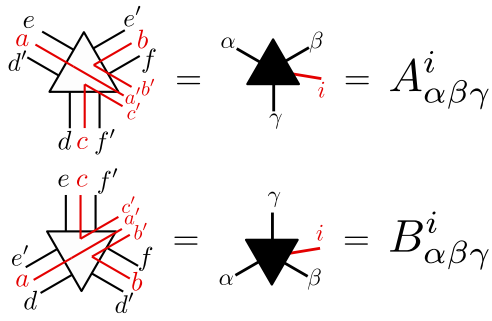

FIG. 5. Tensors forming the iPEPS are defined via combination of F symbols and corresponding quantum dimensions d_i. All bond indices and the physical index are in fact a triple index. The bond dimension can be reduced by applying projectors on the nonzero bond indices.

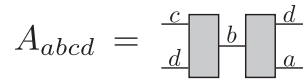

FIG. 6. The tensors A_{abcd} are proportional to $N^b_{da}N^b_{cd}$ and can be represented by the zippers connected by, but not summed over, the index b.

$$A^i_{\alpha\beta\gamma} = \left(\frac{d_a d_b}{d_c}\right)^{1/4} F^{dab}_{fec}\delta_{aa'}\delta_{bb'}\delta_{cc'}\delta_{dd'}\delta_{ee'}\delta_{ff'}, \tag{A1}$$

$$B^i_{\alpha\beta\gamma} = \left(\frac{d_a d_b}{d_c}\right)^{1/4} F^{dab}_{fec}\delta_{aa'}\delta_{bb'}\delta_{cc'}\delta_{dd'}\delta_{ee'}\delta_{ff'}. \tag{A2}$$

By construction, each tensor has a triple of bond indices along each of the three bonds towards nearest-neighbor (NN) lattice sites. We concatenate each triple into a single bond index, e.g., $\alpha = (a, e, d')$. The physical index is also a triple index $i = (a', b', c')$. These basic tensors are forming the topological state after proper contraction of bond indices with respect to their triplet structure. For the toric code and double Fibonacci string nets the bond dimension $D = 2^3 = 8$ is redundantly large and can be reduced to $D = 4$ and 5 after applying projectors on the bond indices, namely, the only nonzero combinations of bond indices (i, j, k) are those, in which the fusion product $i \times j \times k = 1 + \cdots$ contains the trivial anyon. For the double Ising string net, on the other hand, the original bond dimension $D = 3^3 = 27$ can be reduced to $D = 10$.

APPENDIX B: ALGORITHM FOR CENTRAL IDEMPOTENTS

In this Appendix we present an algorithm for numerical calculation of central idempotents from fusion rules N^i_{jk} and F symbols in a random gauge. When inserted into iPEPS, central idempotents can be thought of as projectors onto minimally entangled states. Central idempotents are built from elements A_{abcd}, which form an algebra $\mathcal{A}$ (more precisely it is a C* algebra). The algorithm can be divided into several points as follows.

(i) In the first step we determine all nonzero elements of the algebra $\mathcal{A}$ generated by A_{abcd}:

$$A_{abcd} \propto N^b_{da}N^b_{cd}, \tag{B1}$$

as shown in Fig. 6. Those nonzero elements are the basis vectors of the algebra $\mathcal{A}$, so we can make assignments $e_i = A_{abcd} \neq 0$ and find their multiplication table.

(ii) When treated as matrices in the a, c indices, the multiplication of A_{abcd} satisfies

$$A_{abcd}A_{efah} = e_i e_j = \sum_k f^k_{ij}\, e_k = \sum_k f^k_{ij} A_{encl}. \tag{B2}$$

Using the tensor network diagrammatic expressions, as shown in Fig. 7, we can derive the formula for the structure factors f^k_{ij}, which are given by the F symbols:

$$f^k_{ij} = \sqrt{\frac{d_n d_a d_d d_h}{d_f d_b d_l}} F^{dhe}_{nlf}\left(F^{dah}_{nbf}\right)^{-1} F^{cdh}_{nbl}. \tag{B3}$$

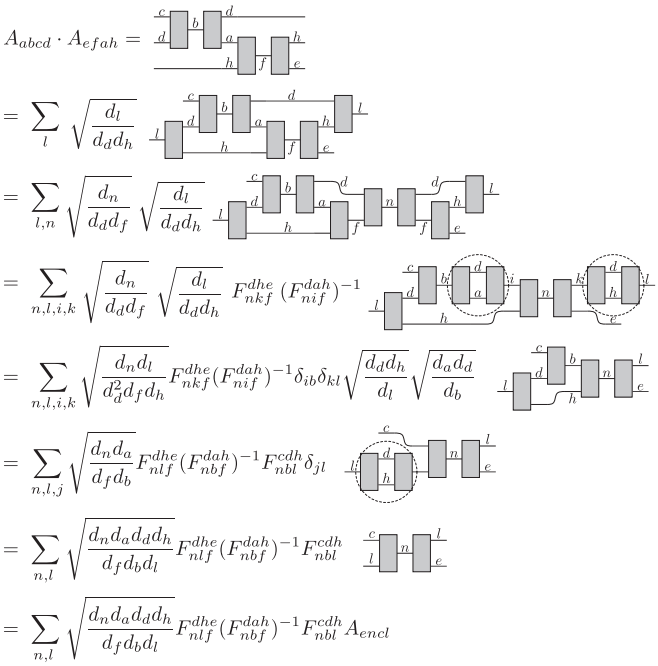

FIG. 7. Derivation of the algebra generated by the tensors A_{abcd} including proper normalization by the quantum dimensions.

(iii) Now we find the center $\mathcal{Z}(\mathcal{A})$ of the algebra $\mathcal{A}$, i.e., we look for such elements $z = \sum_a z_a e_a$ that $\forall\, b:\ ze_b = e_b z$. We observe that this simplifies to an equation involving only the structure factors:

$$\sum_a z_a(e_a e_b - e_b e_a) = 0 \ \Rightarrow\ \forall\, b, c:\ \sum_a \left(f^c_{ab} - f^c_{ba}\right) z_a = 0. \tag{B4}$$

Therefore, the vector of coefficients of z in e_a basis belongs to the kernel of the matrix $\mathcal{F}$: $c(z) := (z_1, \ldots, z_n) \in \mathrm{Ker}(\mathcal{F})$, whose elements are $\mathcal{F}_{b\oplus c,a} = f^c_{ab} - f^c_{ba}$ with $b \oplus c$ index going through all the combinations of b, c indices.

(iv) From now on we work only with the commutative algebra $\mathcal{Z}(\mathcal{A})$, with elements $Z_k = \sum_a z^k_a e_a$, which are linear combinations of the original basis with coefficients from $c(z) \in \mathrm{Ker}(\mathcal{F})$. We construct its adjoint representation, which is given by the structure factors

$$[ad(Z_k)]_{ab} = \sum_c f^b_{ac} z^k_c. \tag{B5}$$

(v) Due to commutation of the elements of the center $\mathcal{Z}(\mathcal{A})$, if we take random element from the center $Z \in \mathcal{Z}(\mathcal{A})$: $Z = \sum_k c_k ad(Z_k)$ and find the transformation bringing it into the diagonal form $U^{-1}ZU$, we know that this transformation is diagonalizing all other elements from the center:

$$\forall\, k:\ U^{-1} ad(Z_k) U = D_k, \tag{B6}$$

where D_k is diagonal.

(vi) We now have to find linear combinations of the matrices D_k to obtain idempotents. Defining d_k as the vectors containing the diagonal elements of D_k, finding idempotents boils down to finding orthogonal linear combinations of the vectors d_k that only contain 1's and 0's. To do this, we build a matrix D with d_k as its row vectors, and compute the row reduced echelon form of the augmented matrix

$$D' = [D \,|\, \mathbb{I}], \quad \mathrm{rref}(D') = [\mathrm{rref}(D) \,|\, M]. \tag{B7}$$

(vii) The central idempotents are now obtained as

$$\mathcal{P}_i = \sum_j M_{ij} Z_j = \sum_{ja} M_{ij} z^j_a e_a. \tag{B8}$$

These central idempotents can be further split into simple idempotents by grouping the different e_a according to the $a = c$ string of the associated tube algebra elements A_{abcd}. We note, however, that this does not always work, as exemplified by the case of Vec_{S_3} in the main text; an alternative general algorithm will be provided in Ref. [76].

[1] X. G. Wen, Topological orders in rigid states, Int. J. Mod. Phys. B **4**, 239 (1990).

[2] A. Kitaev, Fault-tolerant quantum computation by anyons, Ann. Phys. **303**, 2 (2003).

[3] A. Kitaev, Anyons in an exactly solved model and beyond, Ann. Phys. **321**, 2 (2006).

[4] M. A. Levin and X.-G. Wen, String-net condensation: A physical mechanism for topological phases, Phys. Rev. B **71**, 045110 (2005).

[5] Y. Kasahara, T. Ohnishi, Y. Mizukami, O. Tanaka, S. Ma, K. Sugii, N. Kurita, H. Tanaka, J. Nasu, Y. Motome, T. Shibauchi, and Y. Matsuda, Majorana quantization and half-integer thermal quantum hall effect in a kitaev spin liquid, Nature (London) **559**, 227 (2018).

[6] V. Leeb, K. Polyudov, S. Mashhadi, S. Biswas, R. Valentí, M. Burghard, and J. Knolle, Anomalous Quantum Oscillations in a Heterostructure of Graphene on a Proximate Quantum Spin Liquid, Phys. Rev. Lett. **126**, 097201 (2021).

[7] S. R. White, Density Matrix Formulation for Quantum Renormalization Groups, Phys. Rev. Lett. **69**, 2863 (1992).

[8] S. R. White, Density-matrix algorithms for quantum renormalization groups, Phys. Rev. B **48**, 10345 (1993).

[9] S. Yan, D. A. Huse, and S. R. White, Spin-liquid ground state of the $S = 1/2$ kagome Heisenberg antiferromagnet, Science **332**, 1173 (2011).

[10] H.-C. Jiang, Z. Wang, and L. Balents, Identifying topological order by entanglement entropy, Nat. Phys. **8**, 902 (2012).

[11] S.-S. Gong, D. N. Sheng, O. I. Motrunich, and M. P. A. Fisher, Phase diagram of the spin-1/2 $J_1 - J_2$ Heisenberg model on a honeycomb lattice, Phys. Rev. B **88**, 165138 (2013).

[12] Z. Zhu, D. A. Huse, and S. R. White, Weak Plaquette Valence Bond Order in the $S = 1/2$ Honeycomb $J_1 - J_2$ Heisenberg Model, Phys. Rev. Lett. **110**, 127205 (2013).

[13] S.-S. Gong, W. Zhu, and D. N. Sheng, Emergent chiral spin liquid: Fractional quantum Hall effect in a kagome Heisenberg model, Sci. Rep. **4**, 6317 (2014).

[14] Z. Zhu and S. R. White, Quantum phases of the frustrated XY models on the honeycomb lattice, Mod. Phys. Lett. B **28**, 1430016 (2014).

[15] S.-S. Gong, W. Zhu, L. Balents, and D. N. Sheng, Global phase diagram of competing ordered and quantum spin-liquid phases on the kagome lattice, Phys. Rev. B **91**, 075112 (2015).

[16] W.-J. Hu, S.-S. Gong, W. Zhu, and D. N. Sheng, Competing spin-liquid states in the spin-1/2 Heisenberg model on the triangular lattice, Phys. Rev. B **92**, 140403(R) (2015).

[17] W. Zhu, S. S. Gong, D. N. Sheng, and L. Sheng, Possible non-Abelian Moore-Read state in double-layer bosonic fractional quantum Hall system, Phys. Rev. B **91**, 245126 (2015).

[18] Z. Zhu and S. R. White, Spin liquid phase of the $S = 1/2 J_1 - J_2$ Heisenberg model on the triangular lattice, Phys. Rev. B **92**, 041105(R) (2015).

[19] M. P. Zaletel, Z. Zhu, Y.-M. Lu, A. Vishwanath, and S. R. White, Space Group Symmetry Fractionalization in a Chiral Kagome Heisenberg Antiferromagnet, Phys. Rev. Lett. **116**, 197203 (2016).

[20] T.-S. Zeng, W. Zhu, J.-X. Zhu, and D. N. Sheng, Nature of continuous phase transitions in interacting topological insulators, Phys. Rev. B **96**, 195118 (2017).

[21] M.-S. Vaezi and A. Vaezi, Numerical Observation of Parafermion Zero Modes and their Stability in 2D Topological States, arXiv:1706.01192.

[22] Z. Zhu, I. Kimchi, D. N. Sheng, and L. Fu, Robust non-Abelian spin liquid and a possible intermediate phase in the antiferromagnetic Kitaev model with magnetic field, Phys. Rev. B **97**, 241110(R) (2018).

[23] M. Gohlke, G. Wachtel, Y. Yamaji, F. Pollmann, and Y. B. Kim, Quantum spin liquid signatures in kitaev-like frustrated magnets, Phys. Rev. B **97**, 075126 (2018).

[24] M. Gohlke, R. Moessner, and F. Pollmann, Dynamical and topological properties of the kitaev model in a [111] magnetic field, Phys. Rev. B **98**, 014418 (2018).

[25] L. Cincio and G. Vidal, Characterizing Topological Order by Studying the Ground States on an Infinite Cylinder, Phys. Rev. Lett. **110**, 067208 (2013).

[26] Y.-C. He, D. N. Sheng, and Y. Chen, Chiral Spin Liquid in a Frustrated Anisotropic Kagome Heisenberg Model, Phys. Rev. Lett. **112**, 137202 (2014).

[27] W. Zhu, S. S. Gong, F. D. M. Haldane, and D. N. Sheng, Topological characterization of the non-Abelian Moore-Read state using density-matrix renormalization group, Phys. Rev. B **92**, 165106 (2015).

[28] W. Zhu, S. S. Gong, and D. N. Sheng, Chiral and critical spin liquids in a spin-1/2 kagome antiferromagnet, Phys. Rev. B **92**, 014424 (2015).

[29] B. Bauer, L. Cincio, B. P. Keller, M. Dolfi, G. Vidal, S. Trebst, and A. W. W. Ludwig, Chiral spin liquid and emergent anyons in a Kagome lattice Mott insulator, Nat. Commun. **5**, 5137 (2014).

[30] W. Zhu, S. S. Gong, F. D. M. Haldane, and D. N. Sheng, Fractional Quantum Hall States at $\nu = 13/5$ and $12/5$ and Their Non-Abelian Nature, Phys. Rev. Lett. **115**, 126805 (2015).

[31] A. G. Grushin, J. Motruk, M. P. Zaletel, and F. Pollmann, Characterization and stability of a fermionic $\nu = 1/3$ fractional Chern insulator, Phys. Rev. B **91**, 035136 (2015).

[32] Y.-C. He, S. Bhattacharjee, F. Pollmann, and R. Moessner, Kagome Chiral Spin Liquid as a Gauged $U(1)$ Symmetry Protected Topological Phase, Phys. Rev. Lett. **115**, 267209 (2015).

[33] Y.-C. He and Y. Chen, Distinct Spin Liquids and Their Transitions in Spin-1/2 XXZ Kagome Antiferromagnets, Phys. Rev. Lett. **114**, 037201 (2015).

[34] Y.-C. He, S. Bhattacharjee, R. Moessner, and F. Pollmann, Bosonic Integer Quantum Hall Effect in an Interacting Lattice Model, Phys. Rev. Lett. **115**, 116803 (2015).

[35] S. Geraedts, M. P. Zaletel, Z. Papić, and R. S. K. Mong, Competing Abelian and non-Abelian topological orders in $\nu = 1/3 + 1/3$ quantum Hall bilayers, Phys. Rev. B **91**, 205139 (2015).

[36] R. S. K. Mong, M. P. Zaletel, F. Pollmann, and Z. Papić, Fibonacci anyons and charge density order in the 12/5 and 13/5 quantum Hall plateaus, Phys. Rev. B **95**, 115136 (2017).

[37] Y.-C. He, F. Grusdt, A. Kaufman, M. Greiner, and A. Vishwanath, Realizing and adiabatically preparing bosonic integer and fractional quantum Hall states in optical lattices, Phys. Rev. B **96**, 201103(R) (2017).

[38] E. M. Stoudenmire, D. J. Clarke, R. S. K. Mong, and J. Alicea, Assembling Fibonacci anyons from a Z_3 parafermion lattice model, Phys. Rev. B **91**, 235112 (2015).

[39] Y.-C. He, M. P. Zaletel, M. Oshikawa, and F. Pollmann, Signatures of Dirac cones in a DMRG Study of the Kagome Heisenberg Model, Phys. Rev. X **7**, 031020 (2017).

[40] S. N. Saadatmand and I. P. McCulloch, Symmetry fractionalization in the topological phase of the spin-1/2 $J_1 - J_2$ triangular Heisenberg model, Phys. Rev. B **94**, 121111(R) (2016).

[41] C. Hickey, L. Cincio, Z. Papić, and A. Paramekanti, Haldane-Hubbard Mott Insulator: From Tetrahedral Spin Crystal to Chiral Spin Liquid, Phys. Rev. Lett. **116**, 137202 (2016).

[42] M. P. Zaletel, Y.-M. Lu, and A. Vishwanath, Measuring space-group symmetry fractionalization in Z_2 spin liquids, Phys. Rev. B **96**, 195164 (2017).

[43] T.-S. Zeng, W. Zhu, and D. Sheng, Tuning topological phase and quantum anomalous Hall effect by interaction in quadratic band touching systems, npj Quantum Mater. **3**, 49 (2018).

[44] F. Verstraete and J. I. Cirac, Renormalization algorithms for Quantum-Many Body Systems in two and higher dimensions, arXiv:cond-mat/0407066.

[45] V. Murg, F. Verstraete, and J. I. Cirac, Variational study of hard-core bosons in a two-dimensional optical lattice using projected entangled pair states, Phys. Rev. A **75**, 033605 (2007).

[46] F. Verstraete, V. Murg, and J. I. Cirac, Matrix product states, projected entangled pair states, and variational renormalization group methods for quantum spin systems, Adv. Phys. **57**, 143 (2008).

[47] H.-Y. Lee, R. Kaneko, T. Okubo, and N. Kawashima, Gapless Kitaev Spin Liquid to Classical String Gas Through Tensor Networks, Phys. Rev. Lett. **123**, 087203 (2019).

[48] P. Corboz, Variational optimization with infinite projected entangled-pair states, Phys. Rev. B **94**, 035133 (2016).

[49] A. Francuz, J. Dziarmaga, G. Vidal, and L. Cincio, Determining topological order from infinite projected entangled pair states, Phys. Rev. B **101**, 041108(R) (2020).

[50] J.-Y. Chen, L. Vanderstraeten, S. Capponi, and D. Poilblanc, Non-Abelian chiral spin liquid in a quantum antiferromagnet revealed by an iPEPS study, Phys. Rev. B **98**, 184409 (2018).

[51] L. Vanderstraeten, J. Haegeman, P. Corboz, and F. Verstraete, Gradient methods for variational optimization of projected entangled-pair states, Phys. Rev. B **94**, 155123 (2016).

[52] A. Francuz and J. Dziarmaga, Determining non-abelian topological order from infinite projected entangled pair states, Phys. Rev. B **102**, 235112 (2020).

[53] M. B. Şahinoğlu, D. Williamson, N. Bultinck, M. Mariën, J. Haegeman, N. Schuch, and F. Verstraete, Characterizing topological order with matrix product operators, Annales Henri Poincaré **22**, 563 (2021).

[54] N. Bultinck, M. Mariën, D. J. Williamson, M. B. Şahinoğlu, J. Haegeman, and F. Verstraete, Anyons and matrix product operator algebras, Ann. Phys. **378**, 183 (2017).

[55] M. Iqbal, K. Duivenvoorden, and N. Schuch, Study of anyon condensation and topological phase transitions from a Z_4 topological phase using the projected entangled pair states approach, Phys. Rev. B **97**, 195124 (2018).

[56] C. Fernández-González, R. S. K. Mong, O. Landon-Cardinal, D. Pérez-García, and N. Schuch, Constructing topological models by symmetrization: A projected entangled pair states study, Phys. Rev. B **94**, 155106 (2016).

[57] S. P. G. Crone and P. Corboz, Detecting a Z_2 topologically ordered phase from unbiased infinite projected entangled-pair state simulations, Phys. Rev. B **101**, 115143 (2020).

[58] M. Iqbal and N. Schuch, Order Parameters and Critical Exponents for Topological Phase Transitions Through Tensor Networks, Phys. Rev. X **11**, 041014 (2021).

[59] H. He, H. Moradi, and X.-G. Wen, Modular matrices as topological order parameter by a gauge-symmetry-preserved tensor renormalization approach, Phys. Rev. B **90**, 205114 (2014).

[60] J. I. Cirac, D. Pérez-García, N. Schuch, and F. Verstraete, Matrix product density operators: Renormalization fixed points and boundary theories, Ann. Phys. **378**, 100 (2017).

[61] G. De las Cuevas, J. I. Cirac, N. Schuch, and D. Perez-Garcia, Irreducible forms of matrix product states: Theory and applications, J. Math. Phys. **58**, 121901 (2017).

[62] X. Chen, Z.-C. Gu, and X.-G. Wen, Classification of gapped symmetric phases in one-dimensional spin systems, Phys. Rev. B **83**, 035107 (2011).

[63] N. Schuch, D. Pérez-García, and I. Cirac, Classifying quantum phases using matrix product states and projected entangled pair states, Phys. Rev. B **84**, 165139 (2011).

[64] L. Lootens, J. Fuchs, J. Haegeman, C. Schweigert, and F. Verstraete, Matrix product operator symmetries and intertwiners in string-nets with domain walls, SciPost Phys. **10**, 053 (2021).

[65] M. Mignard and P. Schauenburg, Modular categories are not determined by their modular data, Lett. Math. Phys. **111**, 1 (2021).

[66] J. C. Bridgeman, S. T. Flammia, and D. Poulin, Detecting topological order with ribbon operators, Phys. Rev. B **94**, 205123 (2016).

[67] S. Bravyi, M. B. Hastings, and S. Michalakis, Topological quantum order: Stability under local perturbations, J. Math. Phys. **51**, 093512 (2010).

[68] D. J. Williamson, N. Bultinck, and F. Verstraete, Symmetry-enriched topological order in tensor networks: Defects, gauging and anyon condensation, arXiv:1711.07982.

[69] V. Zauner-Stauber, L. Vanderstraeten, M. T. Fishman, F. Verstraete, and J. Haegeman, Variational optimization algorithms for uniform matrix product states, Phys. Rev. B **97**, 045145 (2018).

[70] M. T. Fishman, L. Vanderstraeten, V. Zauner-Stauber, J. Haegeman, and F. Verstraete, Faster methods for contracting infinite two-dimensional tensor networks, Phys. Rev. B **98**, 235148 (2018).

[71] J. Haegeman, K. Van Acoleyen, N. Schuch, J. I. Cirac, and F. Verstraete, Gauging Quantum States: From Global to Local Symmetries in Many-Body Systems, Phys. Rev. X **5**, 011024 (2015).

[72] J. Haegeman, V. Zauner, N. Schuch, and F. Verstraete, Shadows of anyons and the entanglement structure of topological phases, Nat. Commun. **6**, 8284 (2015).

[73] G.-Y. Zhu and G.-M. Zhang, Gapless Coulomb State Emerging from a Self-Dual Topological Tensor-Network State, Phys. Rev. Lett. **122**, 176401 (2019).

[74] T. Lan and X.-G. Wen, Topological quasiparticles and the holographic bulk-edge relation in $(2+1)$-dimensional string-net models, Phys. Rev. B **90**, 115119 (2014).

[75] R. N. C. Pfeifer, G. Evenbly, S. Singh, and G. Vidal, Ncon: A tensor network contractor for matlab, arXiv:1402.0939.

[76] L. Lootens, M. Deweirdt, and F. Verstraete (unpublished).